Journal of Molecular Liquids 371 (2023) 121105

Contents lists available at ScienceDirect

Journal of Molecular Liquids

journal homepage: www.elsevier.com/locate/molliq

Atomistic insights into the microscope mechanism of solid–liquid interaction influencing convective heat transfer of nanochannel

Shuting Yao [a,*], Jiansheng Wang [b,*], Shufeng Jin [a], Fengguang Tan [a], Shuping Chen [a]

[a] School of Petrochemical Engineering, Lanzhou University of Technology, Lanzhou 730050, PR China
[b] School of Mechanical Engineering, Tianjin University, Tianjin 300350, PR China

ARTICLE INFO

Article history:
Received 31 July 2022
Revised 16 December 2022
Accepted 17 December 2022
Available online 20 December 2022

Keywords:
Nanochannel
Convective heat transfer
Solid-liquid interaction
Friction factor
Molecular dynamics

ABSTRACT

Nanochannel cooling technology is widely used in the heat dissipation systems of various micro/-nanoscale electronic devices or components. The consideration of resistance loss and the optimization of heat dissipation are of great significance for the widespread application of nanochannel cooling technology. A model of convective heat transfer in nanochannel with constant wall temperature is established with molecular dynamics method. The effects of solid–liquid interaction on flow and heat transfer characteristics are investigated. The microscopic mechanisms of the solid–liquid interaction influencing heat transfer performance and flow resistance of nanochannel are explored from the atomic level. The results show that the enhancement of the solid–liquid interaction leads to the increases of the coupling degree of vibration frequency between wall and liquid atoms and the orderliness of microstructure of first fluid layer, and finally facilitates heat transfer between nanochannel wall and liquid. The Nusselt number in nanochannel is not a constant and decays exponentially with the increase of temperature jump length. Meanwhile, as the solid–liquid interaction increases, the slip length decreases and the friction factor increases, which are attributed to the augment of the static structure factor, resulting in more fluid atoms in near-wall region are firmly locked by the wall. The friction factor in nanochannel not only depends on the Reynolds number, but also is closely related to the slip length. To further evaluate overall heat transfer performance of the nanochannel that considers flow resistance, the comprehensive performance coefficient is discussed. It's found that the solid–liquid interaction is effective in improving the overall heat transfer performance of the nanochannel within a certain range.

1. Introduction

With the widespread application of micro/nanoscale functional structures, devices and equipments in the fields like industry, electronics, aerospace, bioengineering, medical and information technology [1–4], various micro/nanoscale problems are getting more and more attention today. Among them, the flow and heat transfer at the micro/nanoscale is one of the key concerns. There is a broad background of engineering application of the micro/nanoscale flow and heat transfer, including three-dimensional printed microfluidic devices, microreactors, electrochemical biosensors, and the cooling and heat dissipation of electronic chips [5–7]. Due to the size effect, the flow and heat transfer at the micro/nanoscale exhibits the characteristics that are very different from the conventional scale [8]. Some interfacial phenomena that are usually neglected at the conventional scale such as velocity slip and temperature jump need to be reconsidered [9,10]. In particular, the impacts of these interfacial phenomena derived from the size effect on the flow and heat transfer in confined micro/nano channels or pores deserve in depth study.

For this reason, some experimental studies on slip flow in micro/nanochannel have been conducted [11–13]. It is worth mentioning that the experimental method, especially nanoscale experiment, faces many problems including high processing accuracy of experimental devices, high experimental costs, measuring difficulties and large experimental errors. In contrast to the limitations and difficulties of the nanoscale experiment, molecular dynamics (MD) has the advantage of describing physical process from the atomic level. Meanwhile, the microscopic mechanisms of flow and heat transfer at the nanoscale can also be achieved by MD that do not require continuum assumptions [14–16]. For example, Thompson et al. [17] found that slip length decreased with the increase of solid–liquid interaction, which mainly came from the increase of the microstructure ordering of liquid near the wall. Wang et al. [18] discovered that velocity slip would occur only

* Corresponding authors.
E-mail addresses: yaost@lut.edu.cn (S. Yao), jsw@tju.edu.cn (J. Wang).

https://doi.org/10.1016/j.molliq.2022.121105
0167-7322/

when shear stress was greater than a critical value, and the slip degree depended on the shear stress and surface wetting property. Ren et al. [19] studied the slip behavior of shear flow on the superhydrophobic surface with rectangular groove. It was found that shear stress and slip length were finite in the edge region of the groove, while the shear stress was almost zero and the slip length was infinite in the central region of the gas–liquid interface. By simulating liquid flowing through nanochannel, Toghraie et al. [20] proved that slip length increased with the increasing of the driving force. Hu et al. [21] observed that the dependence of slip on the solid–liquid interaction could be divided into two categories: under the strong solid–liquid interaction, the slip length increased with the decreasing of the solid–liquid interaction. Under the weak solid–liquid interaction, the slip length decreased with the decreasing of the solid–liquid interaction.

Yet, most of current studies on the nanochannel flow just focus on the velocity slip and flow behavior [17–24], and the coupling between flow and heat transfer is overlooked. In many practical engineering applications, the flow and heat transfer in nanochannel are coupled rather than independent. A typical example is a process of convective heat transfer of the nanochannel. Obviously, the velocity slip and flow behavior will inevitably affect interfacial heat transfer of the nanochannel. The investigation on the convective heat transfer in nanochannel is of great practical significance to promote the efficient utilization of nanochannel cooling technology.

Actually, only less attention has been paid to the convective heat transfer of the nanochannel. Chakraborty et al. [25] probed the effects of surface roughness and surface coating on the convective heat transfer in nanochannel. Song et al. [26] studied the influence of surface periodic sinusoidal nanostructures on nanoscale convective heat transfer. Both of them demonstrated that surface rough topology played a positive role in enhancing heat transfer between nanochannel wall and fluid. Besides, the effect of coating properties on the convective heat transfer was investigated in the work of Wang et al. [27]. Their result showed that the coating thickness was very important for heat transfer enhancement and there was an optimal value of coating thickness. Furthermore, the effect of wall material was conducted by Motlagh et al. [28], and they also observed the impact of nanofluids on the convective heat transfer in naochannel [29]. It was found that heat transfer performance was also influenced by nanoparticle morphology and nanoparticle aggregation. In addition, Wang et al. [30] studied the effects of nanopillar cross sectional areas and heights on the flow condensation heat transfer in nanochannel.

Apart from that, solid–liquid interaction is also the key factor affecting flow behavior and interfacial heat transfer, especially when the characteristic size of flow system is dramatically reduced to the nanoscale. In terms of the effect of the solid–liquid interaction on convective heat transfer in nanochannel, Markvoort et al. [31] found that the strong wall-gas interaction had a favorable effect on heat transfer of the nanochannel. Similarly, the result obtained by Ge et al. [32] also revealed that heat transfer enhancement greatly depended on the larger wetting property. The microscopic mechanism of the surface wetting property influencing convective heat transfer was probed by Sun et al. [33] from the perspective of momentum accommodation coefficient. Moreover, the convective heat transfer of water flowing through graphene nanochannel was performed by Marable et al. [34], in which the influence of wall-fluid interaction on heat transfer was also investigated. It has proved that the strong solid–liquid interaction is beneficial for the heat transfer enhancement. In summary, studies mentioned above [25–34] concentrate on the effects of various influencing factors on the heat transfer characteristics in nanochannel.

However, existing studies on the convective heat transfer in nanochannel rarely focus on flow resistance. No effects of various influencing factors on the flow resistance are taken into account. In fact, there is a great increase of the flow resistance because of the significant reduction of characteristic size of the nanochannel. Various influencing factors especially the solid–liquid interaction will also have a significant impact on the flow resistance. Consequently, it will affect the improvement of comprehensive heat transfer performance in nanochannel. Just as reported in the work of Shadloo-Jahromi et al. [35], for water flowing through a rough nanochannel with the superhydrophobic surface, the friction factor in nanochannel was closely related to the solid–liquid interaction. Further, in our previous work [36,37], the effect of surface rough morphology on the flow resistance was explored. It's indicated that only integrating the weak solid–liquid interaction with surface rough morphology, would the comprehensive heat transfer performance considering the flow resistance be better. Then, how the solid–liquid interaction affects the flow resistance in nanochannel? Obviously, the influence mechanism of solid–liquid interaction on the flow resistance needs to be further investigated. Besides, although the vast majority of investigations do indeed demonstrate the influence of solid–liquid interaction on the heat transfer, they suffer from the lack of mechanistic explanation. In particular, it is yet unclear whether the enhancement of heat transfer is derived directly from the augment of the solid–liquid interaction or there are other deeper inducing mechanisms?

In this context, a three-dimensional model of convective heat transfer in nanochannel is established. The effects of solid–liquid interaction on flow and heat transfer characteristics of the nanochannel, including temperature distributions, temperature jump, Nusselt number, velocity distributions, velocity slip and friction factor, will be comprehensively investigated. Then, the microscope mechanisms of the solid–liquid interaction affecting heat transfer and flow resistance in nanochannel are revealed. What's more, the overall heat transfer performance of the nanochannel is assessed by considering heat transfer characteristics and flow resistance jointly.

2. Methodology

2.1. Physical model and simulation method

The computational model of convective heat transfer in nanochannel with the size of L_x = 220 Å, L_y = 43 Å and L_z = 62 Å is illustrated in Fig. 1. Two platinum plates parallel to the *xoy* plane are the solid walls of the nanochannel. Argon atoms act as cold working fluid with the density of 1332 kg/m^3 and there are 9503 atoms in fluid domain with the channel height of H = 50 Å. Each solid wall has a lattice constant of 3.92 Å and there are 3696 platinum atoms. The thickness of each solid wall is 6 Å and wall atoms are arranged following the FCC lattice structure. Considering that the above computational model needs to reflect thermal motion and microstructure of the solid wall, the Einstein solid wall model [38,39] is used in present work. That is, wall atoms do simple harmonic vibration with the same frequency near their lattice sites by using harmonic springs with a spring constant of 179.5 N/m. The convective heat transfer of the nanochannel is achieved based on the thermal pump method [31,32]. As shown in Fig. 1, the fluid domain is divided into three regions: force region, thermostat region and sample region, and x = 0 is located at the entrance of the nanochannel. The force region is located at the x-directional coordinate of -20 Å$<x<$ -12 Å, where the horizontal driving force of 2.4pN along the $\times$ direction is applied to fluid atoms to drive flow. Thermostat region is located inside the region of

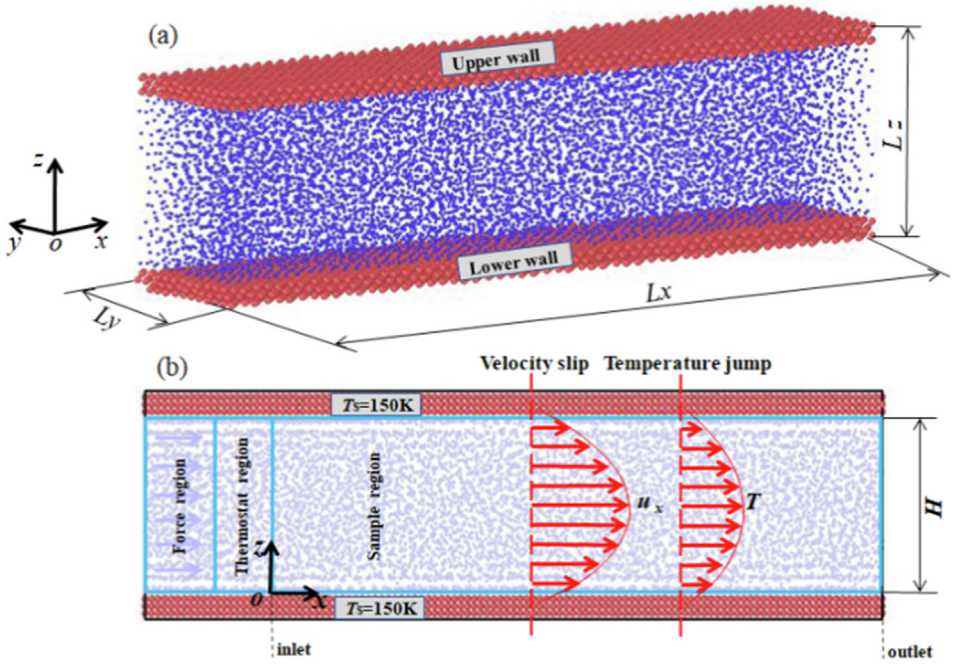

Fig. 1. Calculation model of convective heat transfer in nanochannel.

−12 Å<x < 0 Å, where the temperature of fluid in this region is controlled at 100 K. Then, a process of convective heat transfer in nanochannel can be observed in the sample region of 0 Å<x < 200 Å, accompanying with the fluid inlet initial temperature of 100 K. Meanwhile, the fluid is heated by the channel walls, and the Langevin thermostat method [40,41] is used to keep the temperature of the two parallel channel walls at T_s = 150 K.

All interactions between atoms are described by the well-known Lennard-Jones (LJ) 12–6 potential. The LJ 12–6 potential model is defined as:

$$\phi(r_{ij}) = 4\varepsilon\left[\left(\frac{\sigma}{r_{ij}}\right)^{12} - \left(\frac{\sigma}{r_{ij}}\right)^{6}\right] \tag{1}$$

$$\phi_s(r_{ij}) = 4\varepsilon_s\left[\left(\frac{\sigma_s}{r_{ij}}\right)^{12} - \left(\frac{\sigma_s}{r_{ij}}\right)^{6}\right] \tag{2}$$

$$\phi_{sl}(r_{ij}) = 4\varepsilon_{sl}\left[\left(\frac{\sigma_{sl}}{r_{ij}}\right)^{12} - \left(\frac{\sigma_{sl}}{r_{ij}}\right)^{6}\right] = 4c\sqrt{\varepsilon_s\varepsilon}\left[\left(\frac{\sigma_{sl}}{r_{ij}}\right)^{12} - \left(\frac{\sigma_{sl}}{r_{ij}}\right)^{6}\right] \tag{3}$$

Where ε is the energy parameter, σ denotes the equilibrium distance between atoms when the potential energy is zero. For the interaction between argon atoms, $\varepsilon = \varepsilon_{Ar}$ = 0.01043 eV and $\sigma = \sigma_{Ar}$ = 3.405 Å. For the interaction between platinum atoms, $\varepsilon_s = \varepsilon_{Pt}$ = 0.52 eV and $\sigma_s = \sigma_{Pt}$ = 2.475 Å. For the interaction between platinum and argon atoms, according to the Lorentz-Berthelot rule, the energy parameter $\varepsilon_{PtAr} = \sqrt{\varepsilon_s\varepsilon}$ = 0.0736 eV and $\sigma_{PtAr} = \sigma_{sl}$ = 2.94 Å. As shown in Eq.(3), based on the interaction between platinum and argon atoms ε_{PtAr}, the solid–liquid interaction ε_{sl}, which describes the interaction strength between channel wall atoms and fluid atoms, can be set as different values by tuning the coefficient c to characterize various surface wetting properties. In present work, six coefficients c of 0.025, 0.053, 0.081, 0.142, 0.191 and 0.25 are utilized to probe the influence of the solid–liquid interaction on the flow and heat transfer in nanochannel.

As shown in Fig. 1, a quasi-periodic boundary condition is applied in the x-direction, which is used to guarantee the fluid inlet temperature can be reset accurately only by using the thermal velocity of fluid atoms in thermostat region without affecting the streaming velocity. A periodic boundary condition is applied in the y-direction, while the solid wall boundary condition is used in the z-direction. The time step is 1 fs and the cutoff radius is 10 Å. The Newton's equations of motion are integrated by the Velocity-Verlet algorithm [42,43]. The conjugate gradient (CG) algorithm is used for energy minimization. After the initial configuration is optimized and stabilized by the energy minimization, the NVT ensemble is used to equilibrate the whole system at 100 K for 1.0 ns. To this end, initial velocities of atoms are randomly assigned using the gaussian distribution at 100 K, and the Nosé–Hoover thermostat [44–46] is used to maintain a constant temperature. It could be found that potential energy of the whole system is constantly oscillating around a constant, demonstrating that 1.0 ns is efficient to make the system equilibrium. After the system temperature is stabilized, the non-equilibrium MD simulation driven by the external force is implemented under the NVE ensemble for 8.5 ns. Specifically, the first 0.5 ns is used to make the system reach an equilibrium state with external force, and the subsequent 8.0 ns is used for data acquisition and statistical averaging.

2.2. Governing equations

The local mean fluid temperature $T_m(x)$ over the cross section at different locations along the x direction can be calculated as:

$$T_m(x) = \frac{\int_0^H c_p\rho u_x(x,z)\ T(x,z)dz}{\int_0^H c_p\rho u_x(x,z)dz} \tag{4}$$

Where, c_p is isobaric specific heat capacity, ρ is fluid density. $u_x(x,z)$ is fluid streamwise velocity and $T(x,z)$ is fluid temperature along the x direction.

The local heat transfer coefficient $h(x)$ can be obtained by Eq.(5) and the local Nusselt number Nu_x can be calculated from Eq.(6) as following:

$$h(x) = \frac{\lambda}{(T_s - T_m(x))}\left.\frac{\partial T}{\partial z}\right|_{z=w} \tag{5}$$

$$Nu_x = \frac{h(x)D_h}{\lambda} \tag{6}$$

Where, λ is fluid thermal conductivity, T_s is wall temperature, $\frac{\partial T}{\partial z}|_{z=w}$ is fluid temperature gradient at the solid–liquid interface. D_h is hydraulic diameter, $D_h = 2H$.

Then, the local Nusselt number can be obtained by Eq.(7) as following:

$$Nu_x = \frac{D_h}{(T_s - T_m(x))}\frac{\partial T}{\partial z}\Big|_{z=w} \tag{7}$$

The jump length is usually used to characterize the extent of temperature jump at the solid–liquid interface. The jump length l_k is defined as following:

$$l_k = \frac{\Delta T}{\frac{\partial T}{\partial z}|_{z=w}} \tag{8}$$

Where, ΔT is the temperature jump at the solid–liquid interface. Temperature jump is the difference between fluid temperature at the solid–liquid interface and wall temperature, which can be achieved by extrapolating the fluid temperature profile from fluid to the solid–liquid interface.

The velocity along the x direction can be determined by the Navier–Stokes equation as shown in Eq. (9). Where, μ is shear viscosity of fluid, $\frac{\partial p}{\partial x}$ is pressure gradient along the x direction.

$$\mu\frac{\partial^2 u_x}{\partial z^2} = \frac{\partial p}{\partial x} \tag{9}$$

When the slip boundary is considered, the fluid velocity distribution in nanochannel with the slip boundary condition is as following:

$$u_x = \frac{-(dp/dx)}{2\mu}(-z^2 + Hz) + u_s \tag{10}$$

Where, u_s is slip velocity at the solid–liquid interface, which is the difference between fluid velocity at the solid–liquid interface ($u_x|_{z=w}$) and wall velocity ($u_w = 0$).

The slip length l_s is defined as following:

$$l_s = \frac{u_s}{\frac{\partial u_x}{\partial z}|_{z=w}} \tag{11}$$

Where, $\frac{\partial u_x}{\partial z}|_{z=w}$ is fluid velocity gradient at the solid–liquid interface, which can be obtained by extrapolating the fluid velocity profile to the solid–liquid interface.

Besides, when MD method is used to realize the fluid flow in nanchannel, the flow is driven by applying an external force F_{ext} to each of N fluid atoms in x direction. That is, the magnitude of NF_{ext} corresponds to the $(\Delta p)A$[35,36]. Then, the friction factor f in nanochannel can be computed via the following:

$$f = \frac{\frac{\Delta p}{L_x}D_h}{\frac{1}{2}\rho u_m^2} \tag{12}$$

Where, $\frac{\Delta p}{L_x}$ is pressure gradient along the channel, u_m is fluid mean velocity.

The Colburn factor j can be calculated as Eq.(13), where Re is the Reynolds number and Pr is the Prandtl number.

$$j = \frac{Nu}{RePr^{1/3}} \tag{13}$$

To evaluate overall performance of the nanochannels with different solid–liquid interactions, based on the Colburn factor j and friction factor f, the comprehensive performance coefficient η [47–49] is introduced as shown in Eq.(14). It is taken as an evaluation of the combined hydrodynamic and thermal effects of the nanochannel under the condition of equal flow rate.

$$\eta = \frac{j}{f} = \frac{Nu}{fRePr^{1/3}} \tag{14}$$

In addition, the comprehensive performance coefficient η can also be defined as $j/f^{1/2}$ and $j/f^{1/3}$, respectively, which are used to evaluate the overall heat transfer performance of the nanochannel under the condition of the equal pressure drop and equal pump power, respectively.

3. Validation of numerical model

To verify the reliability and accuracy of the convective heat transfer model in present work, the convective heat transfer in a smooth nanochannel with dimensions of 400 Å×120 Å×60 Å is simulated, and compared with the results obtained by Ref. [32] based on the MD method. Here, the smooth nanochannel consists of two parallel solid walls with Einstein wall model, i.e., the solid wall atoms are connected by a harmonic spring to make simple harmonic vibration at the FCC lattice sites with a spring constant of 70 N/m. The external force driving the fluid flow is 3.4pN and the solid–liquid interaction is 0.01043 eV. The comparison is shown in Fig. 2 for the local Nusselt number along the nanochannel. There is a tiny difference between them, which demonstrates a good agreement with the results in Ref. [32]. Thus, it indicates that the calculation model of convective heat transfer in present work is reliable and accurate.

Moreover, the variation of the difference between wall temperature T_s and fluid mean temperature T_m is shown in Fig. 3(a). It's found that the temperature difference decays exponentially, which is the same as the variation of the temperature difference in conventional channel with constant wall temperature. Under the different solid–liquid interactions, the fluid temperature distributions at the cross section of x = -5.88 Å in nanochannel are presented in Fig. 3(b). It' found that the fluid temperature in the thermostat region could be better controlled at 100 K with a maximum error of no more than 3 %. Therefore, the model of convective heat transfer in nanochannel effectively achieves the control of the fluid inlet temperature, which further validates the reliability of the present numerical model.

In addition, for better evaluating the relationship between the solid–liquid interaction and surface wetting property, MD simula-

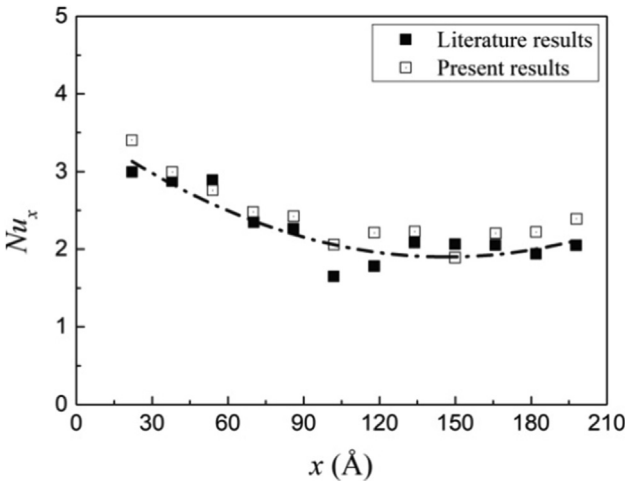

Fig. 2. Comparison of the local Nusselt number between present results and literature results [32].

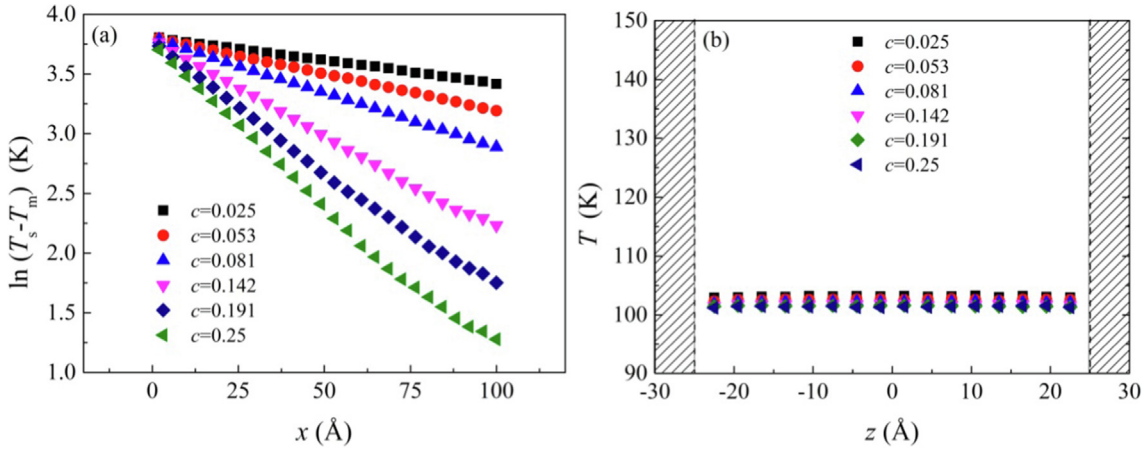

Fig. 3. Mean temperature difference along the flow direction and inlet fluid temperature.

Table 1
Contact angles under different solid–liquid interactions.

Cases	c	$\varepsilon_{sl}/\varepsilon$	Contact angle (MD results)	Contact angle (Equation [50,51])	Contact angle (Wang et al.[52])	Wetting property
1	0.025	0.176	140°	130.3°	115°	weak
2	0.053	0.375	91°	104.5°	/	weak
3	0.081	0.573	47°	81.6°	/	strong
4	0.142	1.0	31°	0°	/	strong
5	0.191	1.348	25°	/	/	strong
6	0.25	1.764	20°	/	26°	stronger

tions for contact angles under different solid–liquid interactions are performed. As shown in Table 1, with the increase of the coefficient c, the solid–liquid interaction ε_{sl} is enhanced and the contact angle θ obtained by MD method gradually decreases, indicating that the surface wetting property is gradually enhanced. The contact angles obtained from MD simulations in present work are in agreement with those of the LJ droplets obtained by empirical equation [50,51] and the results obtained by Wang et al. [52] using MD method. That is, the hydrophilic or hydrophobic characteristic represented by the contact angle is consistent. Simulations of contact angles under different solid–liquid interactions not only quantitatively describe the relationship between the solid–liquid interaction and the surface wetting property, but also verify the reliability of numerical simulation method used in present work.

4. Results and discussions

4.1. Heat transfer characteristics

Under different solid–liquid interactions, the fluid temperature profiles at the same cross section of the nanochannel are shown in Fig. 4. Fig. 4(a) and Fig. 4(b) display the fluid temperature at the cross section of x = 1.96 Å and x = 99.96 Å, respectively. As the fluid is heated, the fluid temperature gradually increases along the flow direction. Yet, for the same cross section, the increase of the fluid temperature depends on the augment of the solid–liquid interaction. It's indicated that strong solid–liquid interaction is conducive to enhance heat exchange between nanochannel wall and fluid. Further, the temperature contours in nanochannels are also shown in Fig. 5. It is clear that the solid–liquid interaction results in significant changes of temperature distributions in nanochannels. Under the same cross section of the nanochannel, the fluid temperature in nanochannel with the strong solid–liquid interaction is higher, which is owing to the intensification of atom collision derived from the strong solid–liquid interaction. However, due to the effect of axial heat conduction caused by the periodic boundary condition in x direction [53], it should be noticed from Fig. 5 that the fluid temperature near the outlet is decreased, just as reported in other literature [31–34]. Therefore, the fluid temperature profiles only at the first half of nanochannel are displayed in Fig. 4, and the flow and heat transfer characteristics in the region far away from the outlet of the nanochannel are discussed in the following.

To explore the heat transfer characteristics of nanochannel, the thermal parameters such as temperature jump length and Nusselt number at the thermally fully developed state are analyzed. It is worth mentioning that when the flow reaches to the thermally fully developed steady state, both velocity profile and temperature profile do no dramatically change along with time, and the temperature profile satisfies the required condition for thermally fully developed flow, i.e.$\frac{\partial}{\partial x}\left[\frac{T_s-T(x,z)}{T_s-T_m(x)}\right]\approx 0$. In present work, a sample region of 41.16 Å<x < 76.44 Å is selected to record thermal and flow parameters at the thermally fully developed state. Fig. 6 shows the effect of the solid–liquid interaction on the temperature jump length and Nusselt number. As shown in Fig. 6(a), with the increase of coefficient c, the normalized temperature jump length $l_k/2H$ gradually decreases and the average Nusselt number gradually increases. The augment of solid–liquid interaction facilitates the reduction of the interfacial temperature jump, which leads to the increases of temperature gradient at the interface and Nusselt number.

The variation of the Nusselt number with the normalized jump length is presented in Fig. 6(b). The red solid line is the fitting relationship between the Nusselt number and the normalized temperature jump length. Here,$Nu = 7.54 - 3.3502(1 - e^{-0.9643\frac{l_k}{2H}}) - 3.8586(1 - e^{-4.4730\frac{l_k}{2H}})$, it's found that the strong dependence of the

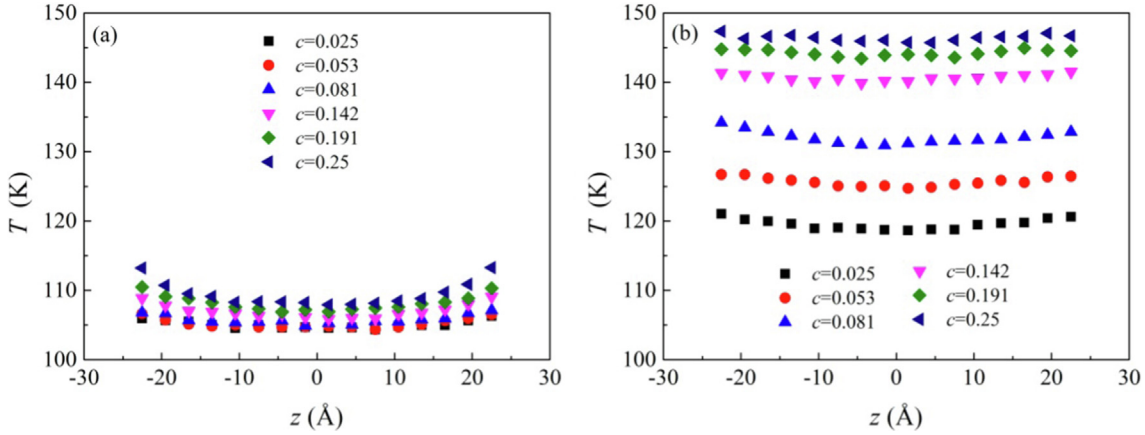

Fig. 4. Temperature profiles at different cross sections in nanochannels.

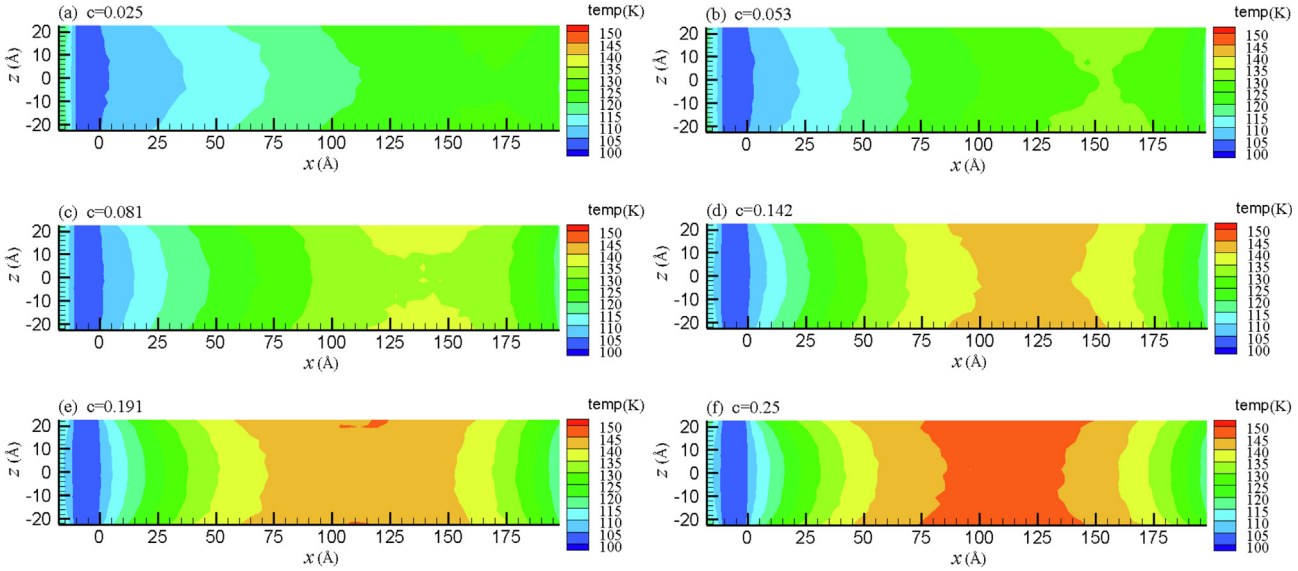

Fig. 5. Temperature distributions in nanochannels under different solid–liquid interactions.

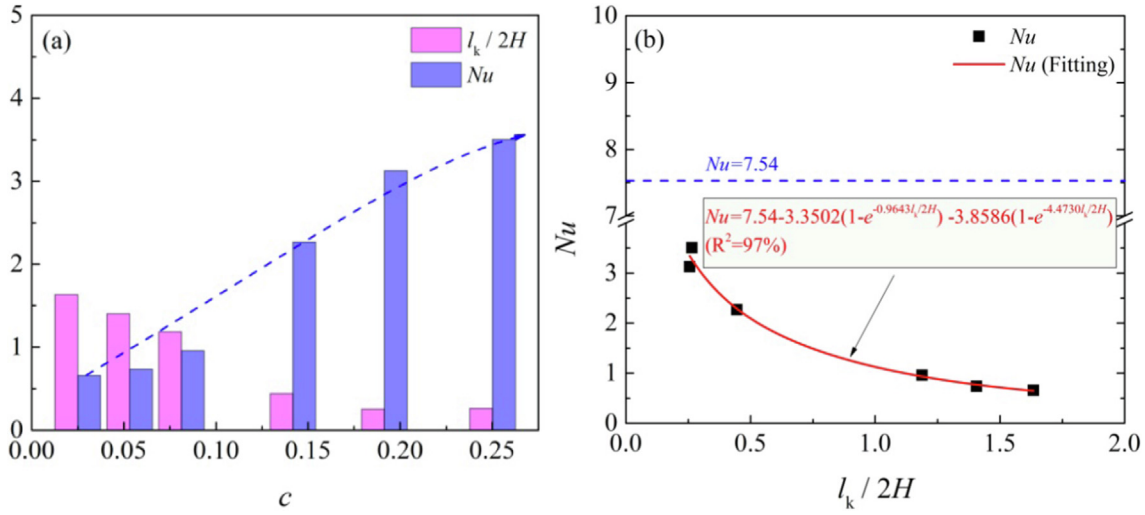

Fig. 6. Effect of solid–liquid interaction on the Nusselt number.

Nusselt number on the interfacial temperature jump. Specifically, the Nusselt number decays exponentially with the increase of the normalized temperature jump length. For a fully developed laminar flow in a conventional parallel-plate channel with constant wall temperature, the corresponding Nusselt number is a constant, i.e., 7.54. However, as shown in Fig. 6(b), the Nusselt number in nanochannel is smaller than 7.54. Based on the above comparison with the conventional scale, it can be concluded that the Nusselt number at the nanoscale depends on the temperature jump directly and is not a constant. When the characteristic size of the nanochannel becomes larger or the temperature jump can be neglected, the Nusselt number gradually approaches 7.54, which is no different from the Nusselt number at the conventional scale. Hence, the existence and significant increase of the temperature jump is an important reason why the Nusselt number at the micro/nanoscale is different from that at the conventional scale.

Several microscope mechanisms of the solid–liquid interaction affecting heat transfer characteristics could be revealed from the perspective of fluid density distributions and vibration coupling between wall atoms and fluid atoms. Fig. 7 depicts the density distributions of fluid under different solid–liquid interactions. The stronger the solid–liquid interaction, the more significant the density layering oscillation near the wall, and the larger the density oscillation amplitude. Consequently, the fluid atoms in layering oscillation region are arranged more closely and orderly by comparing Fig. 7(b) with Fig. 7(c). Then, the fluid atoms are in closer contact with the wall surface, and there are more wall and fluid atoms will participate in heat exchange at per unit contact area. For the convective heat transfer in nanochannel, the heat possessed by the hot channel wall is eventually carried away by thermal conductivity and convection of fluid in the near-wall region. Thus, such tightly ordered microstructure of fluid facilitates the thermal conductivity and reduces the interfacial temperature jump, then enhances the heat transfer. In addition, the density distributions shown in Fig. 7 also demonstrate that the solid–liquid interaction only has a large impact on the fluid layers in the near-wall region, in which the density distribution oscillates significantly. As the distance from the wall surface increases, the effect of channel wall on the density profiles weakens rapidly, the fluid density tends to approach the bulk density. For this reason, the vibration characteristics of fluid atoms in the near-wall region are also investigated in the following.

Actually, many theoretical models [54–59] describing interfacial heat transport have shown that when the heat flows through the solid–liquid interface, the heat carrier (phonon or electron, etc.) will reflect and/or scatter at the interface because of the difference of vibration and other characteristics between two adjacent materials at the interface, then, resulting in the appearance of the interface thermal resistance and hindering the interfacial heat transfer [60,61]. Our previous work [27] has proved that the reduction of coupling degree of vibration frequency between solid wall and liquid atoms derived from the mismatch of atomic properties is the fundamental reason for the increase of interface thermal resistance and temperature jump. Similar conclusions have also been demonstrated in the work of Chakraborty et al [25]. Specifically, the mismatch of vibration characteristics between two different materials can be well quantified by the difference of vibrational density of state (VDOS) [25,62]. The VDOS is obtained by the Fourier transformation of velocity autocorrelation function (VACF) as following:

$$\mathrm{VDOS}\ (\omega) = \int_0^{\tau} \mathrm{VACF}\ (t) e_{-2\pi i\omega t} dt \tag{15}$$

$$\mathrm{VACF}\ (t) = \frac{1}{N}\sum_{i=1}^{N} \frac{\langle \vec{v}_i(t) \cdot \vec{v}_i(0) \rangle}{\langle \vec{v}_i(0) \cdot \vec{v}_i(0) \rangle} \tag{16}$$

Where ω is the angular frequency, $\vec{v}_i$ is the velocity vector of atom i.

The effect of the solid–liquid interaction on the VDOS of wall and fluid atoms is shown in Fig. 8. As the coefficient c increases from 0.025 to 0.25, the solid–liquid interaction becomes stronger. Due to the fact that vibration frequency of fluid atoms in near-wall region moves towards the high frequency, there is a greater coupling of vibration frequency between fluid atoms and wall atoms. The augment of vibration coupling degree leads to a reduction of the interfacial thermal resistance derived from the vibration mismatch between wall atoms and fluid atoms, and thereby is responsible for the enhancement of interfacial heat transfer. The fluid layer adjacent to the channel wall acts as a thermal bridge and promotes thermal transport between the channel wall and the fluid in the mainstream region.

In addition, the solid–liquid interaction will affect the distribution of liquid atoms near the wall, then, the potential energy of liquid atoms is analyzed to reasonably reflect the characteristics of liquid atoms. Meanwhile, considering that the potential energy field of the solid wall surface consists of a series of potential energy peaks and potential energy valleys arranged periodically, the variation of solid–liquid interaction will also affect the potential energy barrier generated by the solid wall, and further affect the condensation and migration of liquid atoms near the wall. Therefore, the potential energy distribution of solid wall atoms is also discussed. Fig. 9 shows the potential energy distribution of liquid atoms at the cross section of z = 22.94 Å under six different solid–liquid interactions, and Fig. 10 displays the potential energy distribution of channel wall atoms at the cross section of z = 25.1

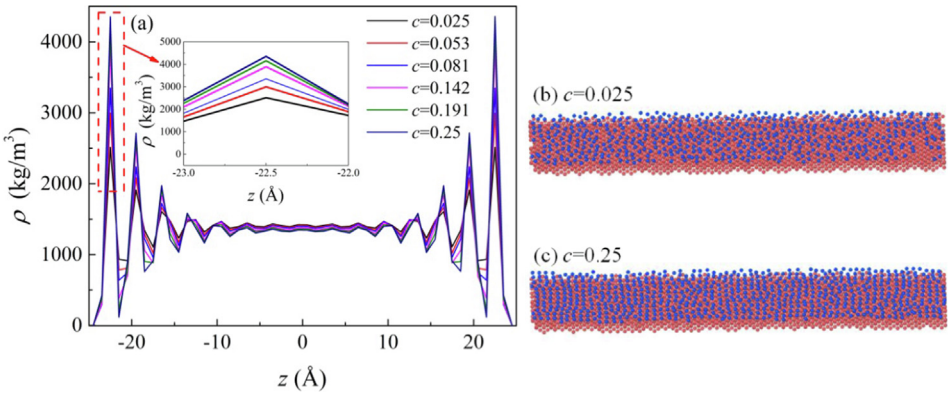

Fig. 7. Effect of solid–liquid interaction on the density profiles.

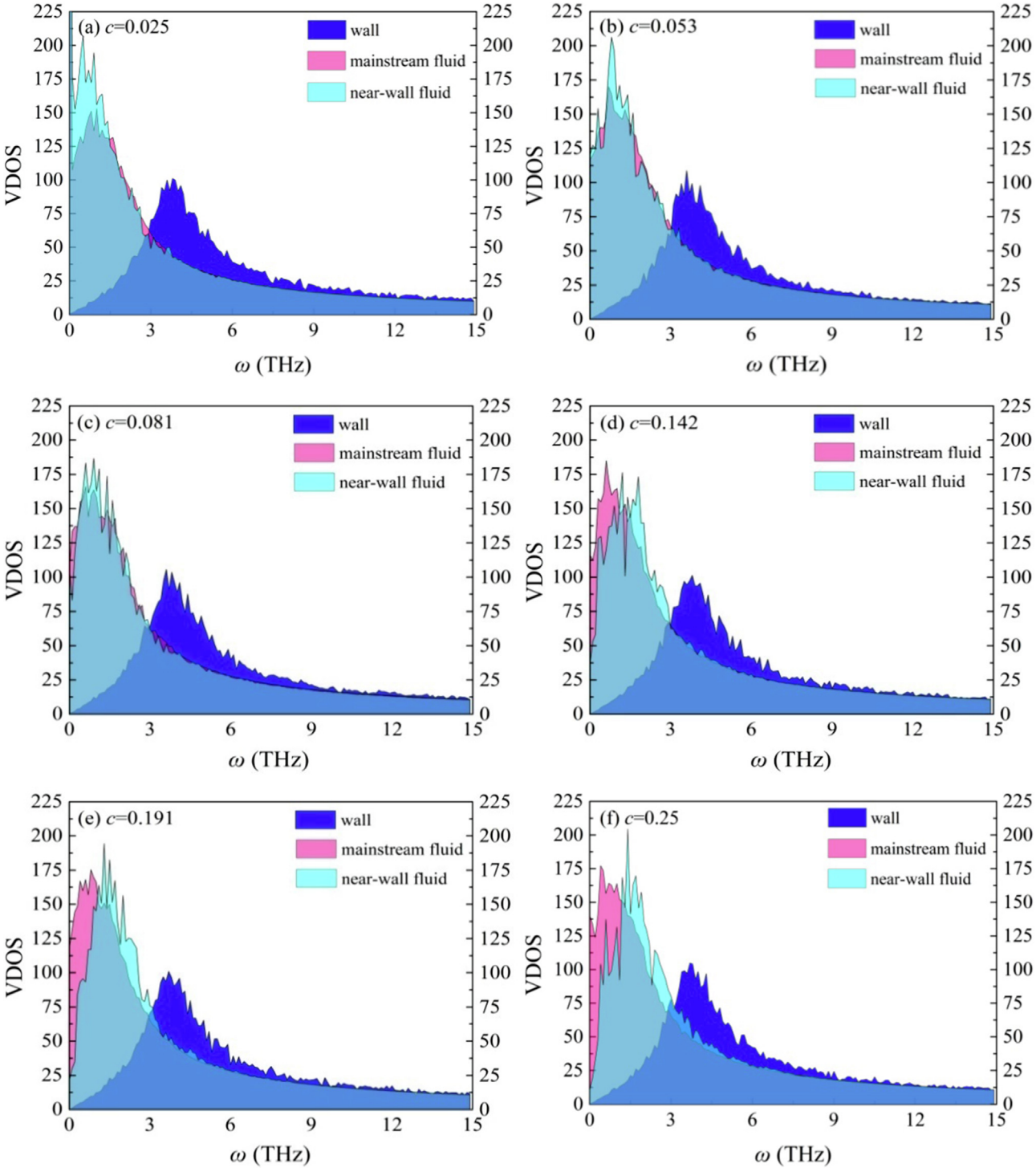

Fig. 8. Effect of solid–liquid interaction on the VDOS of wall and fluid atoms.

96 Å under six different solid–liquid interactions. Here, the region bounded by 55 Å to 65 Å in the *x* direction and 10 Å to 20 Å in the *y* direction on the *xoy* plane is selected as the sample region. By comparing the variations of potential energy distributions of liquid atoms and solid wall atoms as shown in Fig. 9 and Fig. 10 respectively, it's found that the potential energy of liquid atoms and solid wall atoms decreases with the increase of the solid–liquid interaction, but the potential energy of liquid atoms decreases more significantly. As the low potential energy effect of the liquid atoms and channel wall atoms becomes obvious, liquid atoms near the interface are more likely to be trapped in the low potential energy region due to the stronger attraction between wall atoms and liquid atoms. Then, more liquid atoms are involved in the interfacial heat transfer, which is another reason why the strong solid–liquid interaction can enhance heat transfer of the nanochannel.

4.2. Flow resistance characteristics

Fig. 11(a) and Fig. 11(b) show velocity distributions of fluid at the cross section of x = 1.96 Å and x = 99.96 Å, respectively. Along

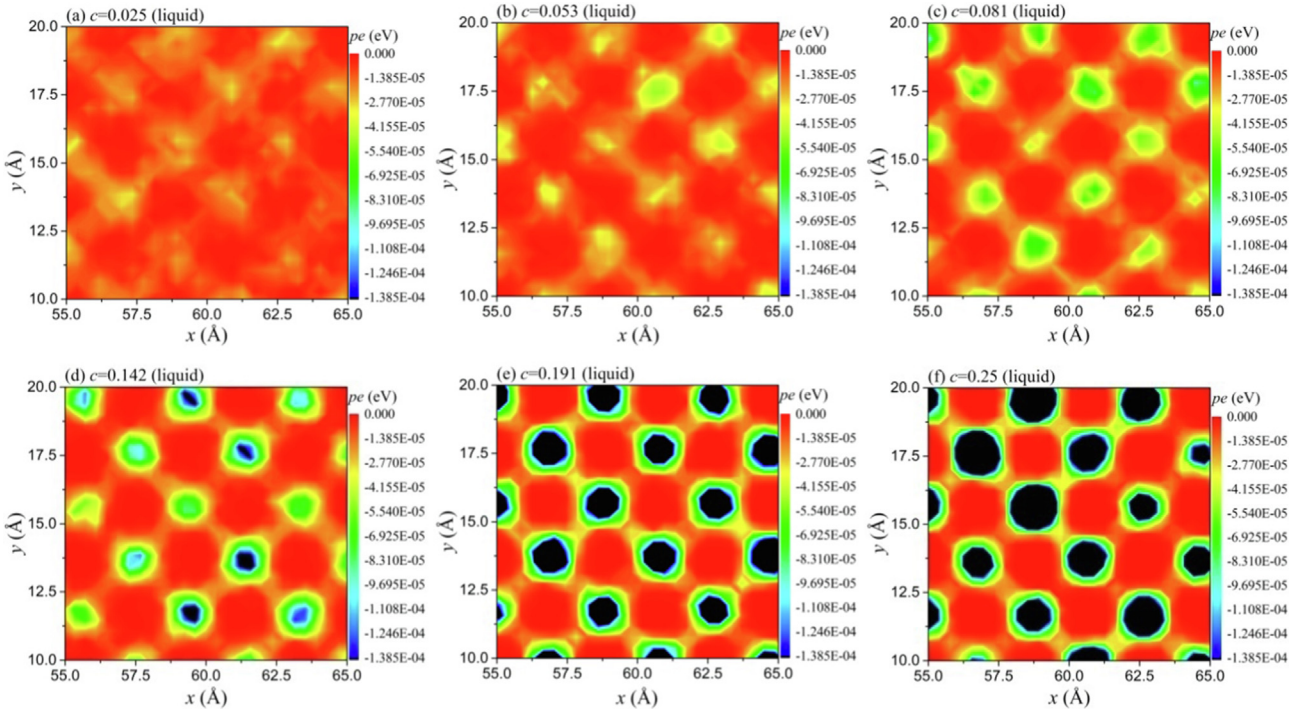

Fig. 9. Distribution of potential energy of liquid atoms.

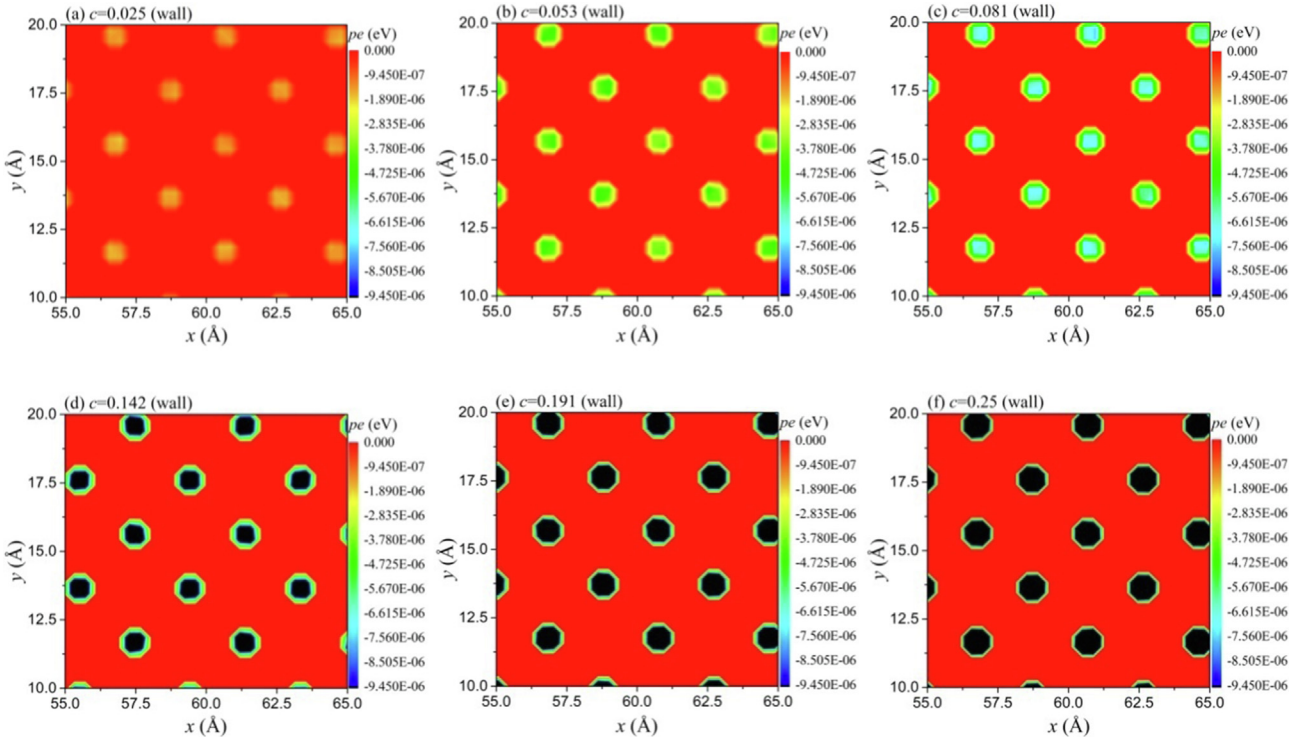

Fig. 10. Distribution of potential energy of solid wall atoms.

the flow direction, the fluid velocity gradually increases. The fluid flow in the nanochannel undergoes a development process and finally reaches a steady state. With the increase of the solid–liquid interaction, the fluid mean velocity at the same cross section is lower. According to the definition of slip velocity, it can be predicted that the more wetting wall surface is not beneficial for the occurrence of the velocity slip and the achievement of drag reduction in nanochannel.

The pressure at specific location along the flow direction under different solid–liquid interactions is shown in Fig. 12. When the solid–liquid interaction is weak, it's found that the nonlinear pressure variation along the flow direction occurs. The pressure gradi-

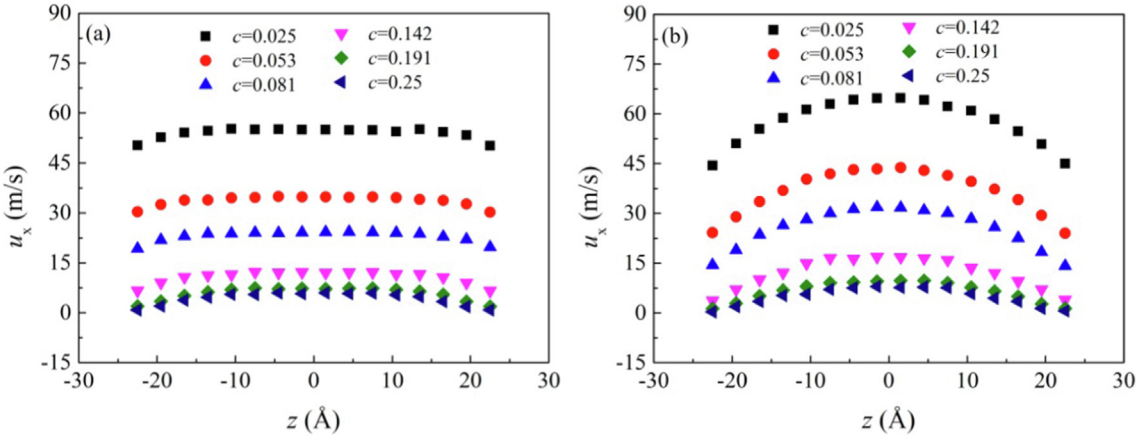

Fig. 11. Velocity profiles at different cross sections in nanochannels.

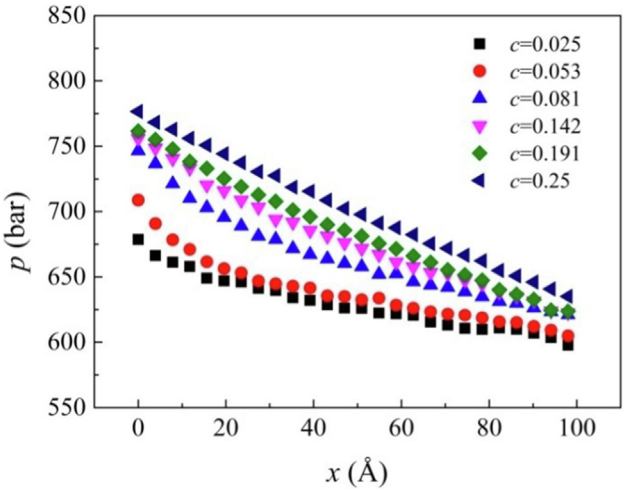

Fig. 12. Variation of the pressure along the *x* direction under different solid–liquid interactions.

ent drops speed in the entrance region and then the pressure drop becomes gentle in the fully developed region, which is attributed to the prominent increase of viscous boundary layer in the entrance region. With the enhancement of solid–liquid interaction, the pressure at the same position becomes higher, the solid–liquid interaction has a greater impact on the pressure than the viscous shearing, which makes the pressure decreases linearly along the flow direction under the same solid–liquid interaction.

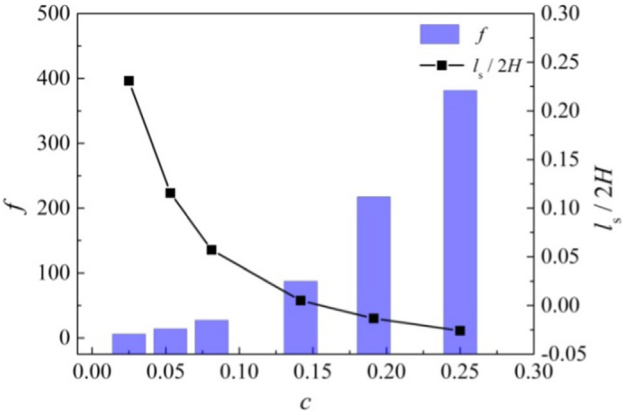

Fig. 13. Effect of solid–liquid interaction on the friction factor.

The variations of friction factor f and normalized slip length $l_s/2H$ in nanochannel with the solid–liquid interaction are presented in Fig. 13, demonstrating that the solid–liquid interaction has a significant effect on the friction factor. When the coefficient c increases from 0.025 to 0.25, the normalized slip length gradually decreases, while the friction factor gradually increases. The variation of the slip length is opposite to the variation of the friction factor, the smaller friction factor is only observed under the weak solid–liquid interaction. Therefore, it indicates that the velocity slip is the direct factor affecting the flow resistance in nanochannel. Increasing the velocity slip is an effective method to the reduction of flow resistance in the nanochannel. To further reveal the mechanism of velocity slip influencing the friction factor, given that velocity slip is closely related to fluid microstructure, then, the microstructure orderliness of the first fluid layer near the wall is analyzed from the perspective of static structure factor (SSF). Here, the first fluid layer refers to the region corresponding to the first density peak adjacent to the solid wall as shown in Fig. 7.

SSF is a statistical physical quantity reflecting the structural disorderliness quantitatively and the expression is as following: $S(\vec{k}) = \frac{1}{N}\left|\sum_{j=1}^{N} \exp(i\vec{k}\cdot\vec{r}_j)\right|^2$. Where N is the total number of liquid atoms in the first fluid layer, $\vec{r}_j$ is the two-dimensional position vector of the jth liquid atom, $\vec{r}_j = (x_j, y_j)$, $\vec{k}$ is the inverse lattice vector parallel to the channel wall (i.e. *xoy* plane), $\vec{k} = (k_x, k_y)$. Here, k_x and k_y are set as an integral multiple of $2\pi/L$, L is the size of the simulation system in the x and y directions, L_x = 200 Å, L_y = 43 Å. The time interval for sampling the position information of liquid atoms in the first fluid layer near the wall is 1×10^4 time steps. The larger the SSF, the more orderly the fluid microstructure, the more obvious the solid-like property. Fig. 14 shows the distributions of the SSF of the first fluid layer near the wall. When the solid–liquid interaction is weak (c = 0.025), the fluid microstructure in the near-wall region shows a disorderly state, and the main peak value of the SSF is small. With the increase of the solid–liquid interaction, there are more spikes of the SSF and the mean peak value gradually increases. This phenomenon indicates that the microstructure orderliness of the first fluid layer increases. Furthermore, under the stronger solid–liquid interaction, i.e. c = 0.25, the microstructure of the first fluid layer obeys solid-like nature obviously and the nonconformity of microstructure between channel wall and first fluid layer decreases. As a result, the fluid layer in the near-wall region will be firmly locked by the solid wall, which is not conducive to the occurrence of velocity

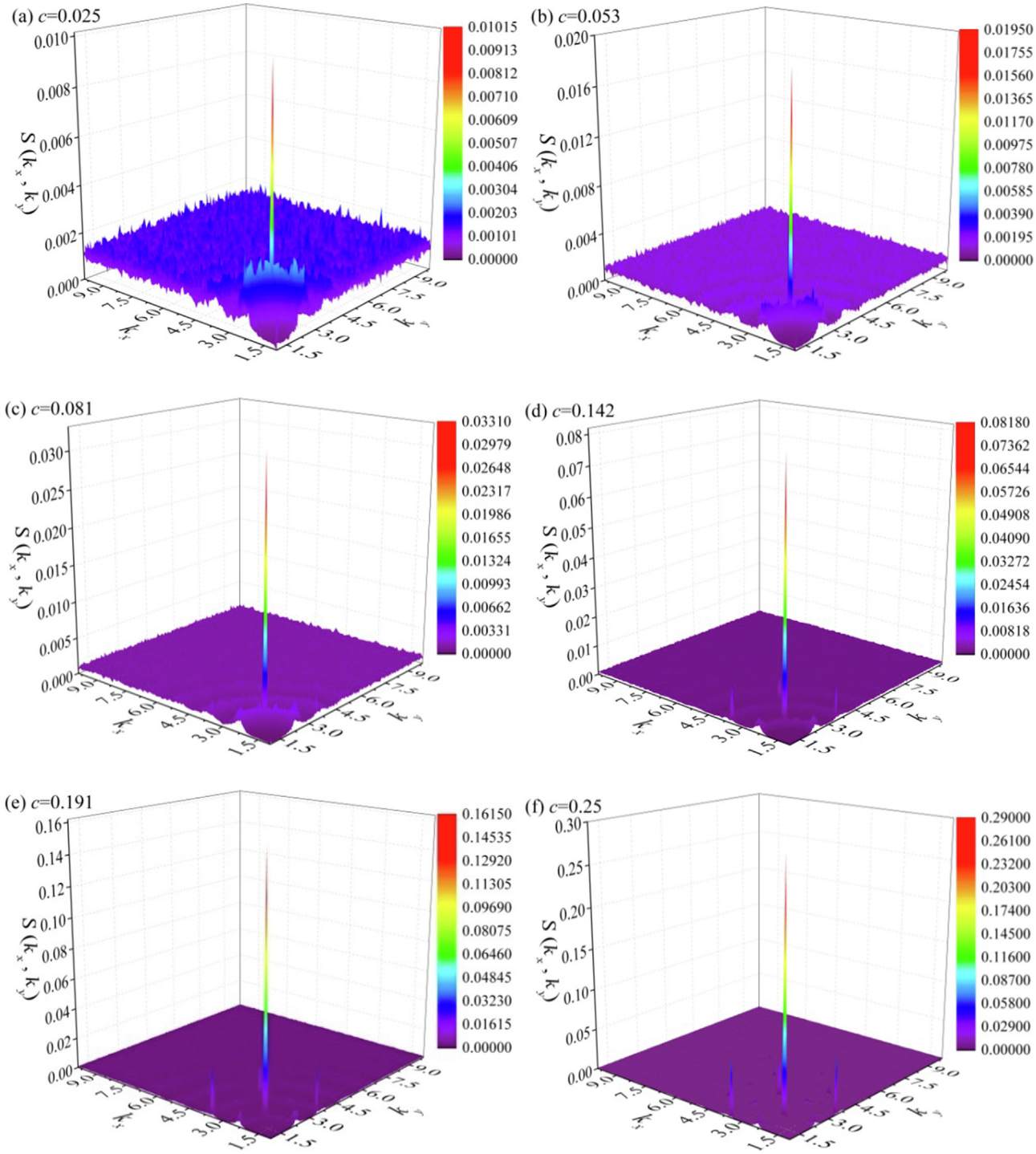

Fig. 14. Variation of the static structure factor with the solid–liquid interaction.

slip, and even leads to negative slip, thus hindering the movement of fluid atoms and causing a significant increase of the friction factor.

Just as shown in Fig. 15, the normalized slip length decreases significantly with the increasing of the mean peak value of the SSF, which is consistent with the result that slip velocity is negatively correlated with the SSF as elaborated in the literature [17]. Therefore, the velocity slip is directly related to the fluid microstructure in the near-wall region, especially the first fluid layer. The increase of the SSF is the fundamental reason why the friction factor increases with the augment of the solid–liquid interaction.

Current studies on the flow resistance characteristics in microchannels have shown that the product of friction factor and Reynolds number (*fRe*) is either higher or lower than the value in conventional channels [8,63]. Although the results are not uniform, they are sufficient to convince that there are differences of flow resistance characteristics between micro/nanochannels and conventional channels. The variation of the friction factor with Reynolds number under different solid–liquid interactions is shown

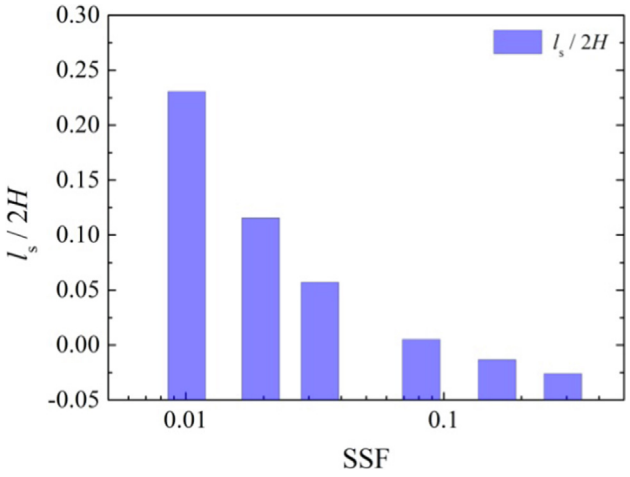

Fig. 15. Variation of the slip length with the static structure factor.

in Fig. 16 (a). It's found that the friction factor in the nanochannel appears a non-linear decreasing trend with the increasing of the Reynolds number, which is consistent with the variation of friction factor in microchannels obtained by Mohiuddin Mala et al. [64]. Meanwhile, the friction factor in nanochannel is significantly different from that in conventional channel, in which the product of the friction factor and the Reynolds number is a constant for fully developed laminar flow, i.e. fRe = 96. Such nonlinear variation of the friction factor with Reynolds number can be explained from the effect of velocity slip. The variation of the product (fRe) with the normalized slip length is demonstrated in Fig. 16(b), where the product of fRe decreases with the increase of the normalized slip length. The red solid line in the figure is the fitting relationship of the product (fRe) as a function of slip length. Specifically, $fRe = \frac{96}{1+13.63\frac{l_s}{2H}}$. When there is slip, $l_s > 0$ and $fRe < 96$. When there is no slip, i.e. $l_s = 0$, fRe approaches the value in conventional channel and fRe = 96. When it is adherent or negative slip boundary condition, $l_s < 0$ and $fRe > 96$. Hence, compared with the conven-

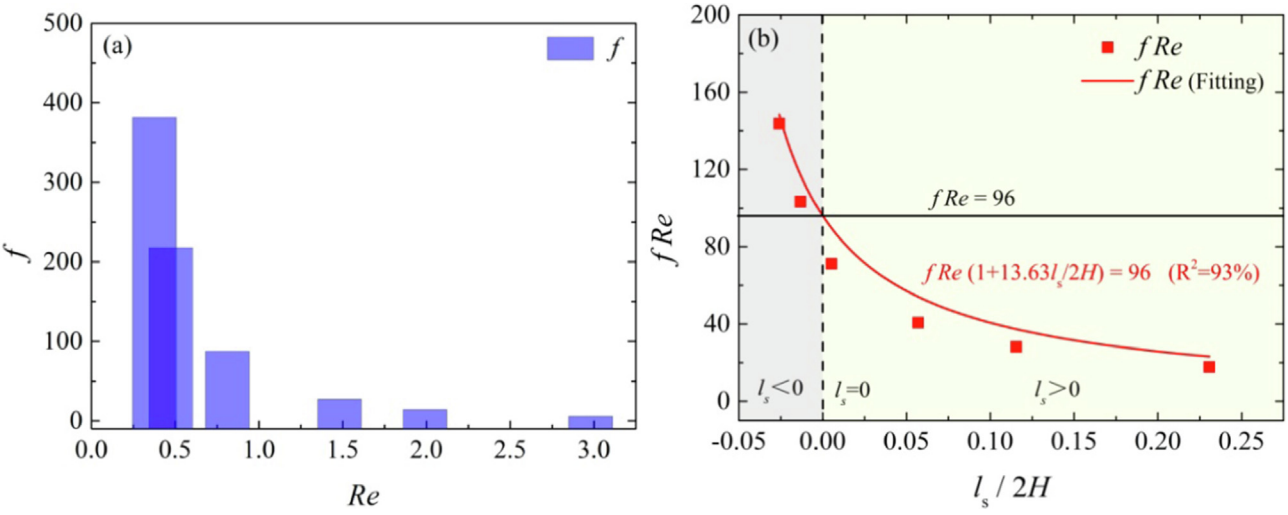

Fig. 16. Relationship between the friction factor and the slip length.

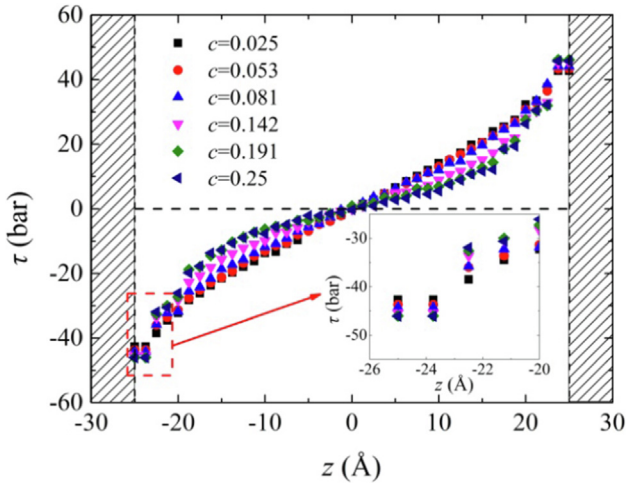

Fig. 17. Variation of the shear stress with the solid–liquid interaction.

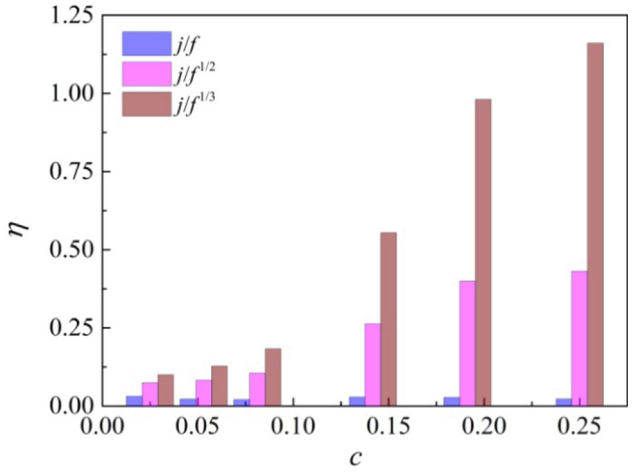

Fig. 18. Variation of the comprehensive performance coefficient with the solid–liquid interaction.

tional channel, the friction factor in the nanochannel is not only related to the Reynolds number, but also closely depends on the degree of the interfacial slip.

Besides, the variation of shear stress with the solid–liquid interaction is given in Fig. 17, showing that fluid shear stress and stress gradient near the wall gradually increase with the enhancement of solid–liquid interaction. Thus, it further verifies that the velocity gradient at the solid–liquid interface gradually increases, which is consistent with the result that the interfacial slip decreases with the augment of the solid–liquid interaction.

As shown in Fig. 6(a) and Fig. 13, both the Nusselt number and the friction factor increase with the augment of the solid–liquid interaction. Hence, in the following, the overall heat transfer performance of the nanochannel is evaluated by the comprehensive performance coefficient η. As shown in Fig. 18, η first increases with the increase of coefficient c, when the coefficient c varies from 0.081 to 0.142, η increases significantly. At this point, an increase rate of 75 % of the coefficient c leads to an increase of 203 % for $j/f^{1/3}$, 150 % for $j/f^{1/2}$ and 40 % for j/f, respectively. As the coefficient c increases to 0.191, the increasing trend of η tends to slow down gradually. This phenomenon fully indicates that adjusting solid–liquid interaction is effective in improving overall heat transfer performance of the nanochannel within a certain range of the solid–liquid interaction. If the solid–liquid interaction continues to increase, the improvement of the overall heat transfer performance of nanochannel will be weakened by the significant increase of the flow resistance.

5. Conclusions

In present work, the solid–liquid interaction that could be significantly responsible for the interfacial heat transfer in nanochannel is considered, and the effects of the solid–liquid interaction on flow and heat transfer characteristics in nanochannel are investigated. The microscopic mechanisms capable of explaining the solid–liquid interaction affecting flow resistance and heat transfer performance are revealed, which provides a new insight for the effect of solid–liquid interaction. The main conclusions are as following:

(1) With the enhancement of the solid–liquid interaction, the microstructure orderliness of the first fluid layer near the wall increases, the number of fluid atoms involved in heat exchange at per unit contact area increases. Meanwhile, the coupling of vibration frequency between wall atoms and fluid atoms increases. Consequently, the heat transfer at the solid–liquid interface is enhanced.

(2) A fitting relationship between Nusselt number and temperature jump length is established. It's found that the Nusselt number in nanochannel is not a constant and decays exponentially with the decrease of solid–liquid interaction. Furthermore, the existence and increase of interfacial temperature jump is an important reason why the Nusselt number at the micro/nanoscale is different from that at the conventional scale.

(3) As the solid–liquid interaction increases, the main peak value of SSF of the first fluid layer increases and the solid-like nature of the first fluid layer becomes obvious, which leads to the decrease of slip length. A relationship between fRe and normalized slip length is proposed and confirms that the decrease of velocity slip caused by the increase of SSF is the fundamental reason for the increase of friction factor, which provides a new perspective on the reason why nanoscale flow characteristics are different from that at the conventional scale.

(4) The comprehensive performance coefficient first increases significantly and then tends to slow down with the increase of solid–liquid interaction, which indicates that the solid–liquid interaction effectively improves the overall heat transfer performance within a certain range. If the solid–liquid interaction continues to increase, the significant increase of flow resistance will weaken the improvement of overall heat transfer performance of the nanochannel.

CRediT authorship contribution statement

Shuting Yao: Investigation, Methodology, Software, Validation, Writing – original draft, Visualization. **Jiansheng Wang:** Conceptualization, Writing – review & editing. **Shufeng Jin:** Software, Funding acquisition. **Fengguang Tan:** Data curation, Validation. **Shuping Chen:** Funding acquisition.

Data availability

The data that has been used is confidential.

Declaration of Competing Interest

The authors declare that they have no known competing financial interests or personal relationships that could have appeared to influence the work reported in this paper.

Acknowledgments

The authors gratefully acknowledge the financial support by the National Natural Science Foundation of China (Grant No.52163033) and the Province Nature Science Foundation of Gansu (Grant No.21JR7RA269).

References

[1] A. Skardal, S.V. Murphy, M. Devarasetty, et al., Multi-tissue interactions in an integrated three-tissue organ-on-a-chip platform, Sci. Rep. 7 (1) (2017) 1–16.
[2] H.E. Ahmed, B.H. Salman, A.S. Kherbeet, et al., Optimization of thermal design of heat sinks: A review, Int. J. Heat Mass Transf. 118 (2018) 129–153.
[3] A.K. Basu, A. Basu, S. Bhattacharya, Micro/nano fabricated cantilever based biosensor platform: A review and recent progress, Enzyme Microb. Technol. 139 (2020).
[4] Y. Li, Q. Zhang, Y. Liu, et al., Regulation of nanocrystals structure for high-performance magnetic triboelectric nanogenerator, Nano Energy 89 (2021).
[5] M. Bhaiyya, P.K. Pattnaik, S. Goel, A brief review on miniaturized electro chemiluminescence devices: From fabrication to applications, Curr. Opin. Electrochem. 30 (2021).
[6] L. Liu, S. Choi, Miniature microbial solar cells to power wireless sensor networks, Biosens. Bioelectron. 177 (2021).
[7] T. Wei, H. Oprins, V. Cherman, et al., Experimental and numerical study of 3D printed direct jet impingement cooling for High-Power, large die size applications, IEEE Trans. Compon. Packag. Manuf. Technol. 11 (3) (2021) 415–425.
[8] Z. Guo, Z. Li, Size effect on microscale single-phase flow and heat transfer, Int. J. Heat Mass Transf. 46 (1) (2003) 149–159.
[9] S. Yao, J. Wang, X. Liu, Influence of nanostructure morphology on the heat transfer and flow characteristics in nanochannel, Int. J. Therm. Sci. 165 (2021).
[10] X. Yong, L.T. Zhang, Slip in nanoscale shear flow: Mechanisms of interfacial friction, Microfluid. Nanofluid. 14 (1–2) (2013) 299–308.
[11] C. Choi, K.J.A. Westin, K.S. Breuer, Apparent slip flows in hydrophilic and hydrophobic microchannels, Phys. Fluids 15 (10) (2003) 2897.
[12] L. Li, J. Mo, Z. Li, Flow and slip transition in nanochannels, Phys. Rev. E 90 (3) (2014) 33003.
[13] K. Chen, Q. Li, T. Omori, et al., Slip length measurement in rectangular graphene nanochannels with a 3D flow analysis, Carbon 189 (2022) 162–172.
[14] N. Wu, L. Zeng, T. Fu, et al., Mechanism of heat transfer enhancement by nanochannels copper plate interface wettability: A molecular dynamics study, Int. J. Therm. Sci. 159 (2021).
[15] W. Wang, S. Huang, X. Luo, MD simulation on nano-scale heat transfer mechanism of sub-cooled boiling on nanao-strctured surface, Int. J. Heat Mass Transf. 100 (2016) 276–286.
[16] F. Zhang, X. Jiang, G. Chen, et al., Electric-Field-Driven ion emission from the free surface of room temperature ionic liquids, The Journal of Physical Chemistry Letters 12 (1) (2021) 711–716.
[17] P.A. Thompson, M.O. Robbins, Shear flow near solids: Epitaxial order and flow boundary conditions, Phys. Rev. A 41 (12) (1990) 6830–6837.

[18] F. Wang, Y. Zhao, Slip boundary conditions based on molecular kinetic theory: The critical shear stress and the energy dissipation at the liquid-solid interface, Soft Matter 7 (18) (2011) 8628.
[19] L. Ren, H. Hu, L. Bao, et al., Many-body dissipative particle dynamics study of the local slippage over superhydrophobic surfaces, Phys. Fluids 33 (7) (2021) 72001.
[20] D. Toghraie Semiromi, A.R. Azimian, Nanoscale Poiseuille flow and effects of modified Lennard-Jones potential function, Heat Mass Transf. 46 (7) (2010) 791–801.
[21] H. Hu, L. Bao, N.V. Priezjev, et al., Identifying two regimes of slip of simple fluids over smooth surfaces with weak and strong wall-fluid interaction energies, J. Chem. Phys. 146 (3) (2017) 34701.
[22] H. Noorian, D. Toghraie, A.R. Azimian, Molecular dynamics simulation of Poiseuille flow in a rough nano channel with checker surface roughnesses geometry, Heat Mass Transf. 50 (1) (2014) 105–113.
[23] A.E. Giannakopoulos, F. Sofos, T.E. Karakasidis, et al., Unified description of size effects of transport properties of liquids flowing in nanochannels, Int. J. Heat Mass Transf. 55 (19–20) (2012) 5087–5092.
[24] F. Sofos, T.E. Karakasidis, A.E. Giannakopoulos, et al., Molecular dynamics simulation on flows in nano-ribbed and nano-grooved channels, Heat Mass Transf. 52 (1) (2016) 153–162.
[25] P. Chakraborty, T. Ma, L. Cao, et al., Significantly enhanced convective heat transfer through surface modification in nanochannels, Int. J. Heat Mass Transf. 136 (2019) 702–708.
[26] Z. Song, Z. Cui, Q. Cao, et al., Molecular dynamics study of convective heat transfer in ordered rough nanochannels, J. Mol. Liq. 337 (2021).
[27] S. Yao, J. Wang, X. Liu, The influence of wall properties on convective heat transfer in isothermal nanochannel, J. Mol. Liq. 324 (2021).
[28] M. Bagheri Motlagh, M. Kalteh, Investigating the wall effect on convective heat transfer in a nanochannel by molecular dynamics simulation, Int. J. Therm. Sci. 156 (2020).
[29] M. Bagheri Motlagh, M. Kalteh, Molecular dynamics simulation of nanofluid convective heat transfer in a nanochannel: Effect of nanoparticles shape, aggregation and wall roughness, J. Mol. Liq. 318 (2020).
[30] M. Wang, H. Sun, L. Cheng, Flow condensation heat transfer characteristics of nanochannels with nanopillars: A molecular dynamics study, Langmuir 37 (50) (2021) 14744–14752.
[31] A.J. Markvoort, P.A. Hilbers, S.V. Nedea, Molecular dynamics study of the influence of wall-gas interactions on heat flow in nanochannels, Phys. Rev. E 71 (6 Pt 2) (2005) 66702.
[32] S. Ge, Y. Gu, M. Chen, A molecular dynamics simulation on the convective heat transfer in nanochannels, Mol. Phys. 113 (7) (2015) 703–710.
[33] H. Sun, Z. Liu, G. Xin, et al., Thermal and flow characterization in nanochannels with tunable surface wettability: A comprehensive molecular dynamics study, Numer. Heat Transfer, Part A: Appl. 78 (6) (2020) 231–251.
[34] D.C. Marable, S. Shin, N.A. Yousefzadi, Investigation into the microscopic mechanisms influencing convective heat transfer of water flow in graphene nanochannels, Int. J. Heat Mass Transf. 109 (2017) 28–39.
[35] A. Shadloo-Jahromi, M. Kharati-Koopaee, O. Bavi, Molecular dynamics simulation of fluid flow through nanochannels consisting of different superhydrophobic patterns, Int. Commun. Heat Mass Transfer 124 (2021).
[36] S. Yao, J. Wang, X. Liu, Role of wall-fluid interaction and rough morphology in heat and momentum exchange in nanochannel, Appl. Energy 298 (2021).
[37] S. Yao, J. Wang, X. Liu, The impacting mechanism of surface properties on flow and heat transfer features in nanochannel, Int. J. Heat Mass Transf. 176 (2021).
[38] P.A. Thompson, S.M. Troian, A general boundary condition for liquid flow at solid surfaces, Nature 389 (6649) (1997) 360–362.
[39] J. Sun, Z. Li, Three-Dimensional molecular dynamic study on accommodation coefficients in rough nanochannels, Heat Transfer Eng. 32 (7–8) (2011) 658–666.
[40] T. Schneider, E. Stoll, Molecular-dynamics study of s three-dimensional one-component model for distortive phase transitions, Phys. Rev. B 17 (3) (1978) 1302–1322.
[41] S. Lepri, R. Livi, A. Politi, Thermal conduction in classical low-dimensional lattices, Phys. Rep. 377 (2003) 1–80.
[42] V.L. Computer, "Experiments" on Classical Fluids. I. Thermodynamical Properties of Lennard-Jones Molecules, Phys. Rev. 159 (1) (1967) 98–103.
[43] G.J. Martyna, M.E. Tuckerman, D.J. Tobias, et al., Explicit reversible integrators for extended systems dynamics, Mol. Phys. 87 (5) (1996) 1117–1157.
[44] S. Nose, A unified formulation of the constant temperature molecular dynamics methods, J. Chem. Phys. 81 (1) (1984) 511–519.
[45] W.G. Hoover, Canonical dynamics: Equilibrium phase-space distributions, Physics Review A 31 (3) (1985) 1695–1697.
[46] G.J. Martyna, M.L. Klein, M. Tuckerman, Nose-Hoover chains: The canonical ensemble via continuous dynamics, J. Chem. Phys. 97 (4) (1992) 2635–2643.
[47] A.L. London, Compact heat exchanger. ASME, Mech. Eng. 86 (1964) 31–34.
[48] J. Lee, K. Lee, Friction and Colburn factor correlations and shape optimization of chevron-type plate heat exchangers, Appl. Therm. Eng. 89 (2015) 62–69.
[49] Y. Cheng, J. Xu, Y. Sui, Numerical study on drag reduction and heat transfer enhancement in microchannels with superhydrophobic surfaces for electronic cooling, Appl. Therm. Eng. 88 (2015) 71–81.
[50] P.G. de Gennes, Wetting: Statics and dynamics, Review of Modern Physics 57 (3) (1985) 827–863.
[51] J.B. Freund, The atomic detail of a wetting/de-wetting flow, Phys. Fluids 15 (5) (2003) L33–L36.
[52] M. Wang, H. Sun, L. Cheng, Investigation of convective heat transfer performance in nanochannels with fractal Cantor structures, Int. J. Heat Mass Transf. 171 (2021).
[53] Y. Gu, S. Ge, M. Chen, A molecular dynamics simulation of nanoscale convective heat transfer with the effect of axial heat conduction, Mol. Phys. 114 (12) (2016) 1922–1930.
[54] P. Zhang, P. Yuan, X. Jiang, et al., A theoretical review on interfacial thermal transport at the nanoscale, Small 14 (2) (2018) 1702769.
[55] D.G. Cahill, P.V. Braun, G. Chen, et al. Nanoscale thermal transport. II. 2003–2012. Appl. Phys. Rev., 2014, 1(1): 11305.
[56] H. Zhou, G. Zhang, General theories and features of interfacial thermal transport, Chin. Phys. B 27 (3) (2018) 34401.
[57] A. Giri, P.E. Hopkins, A review of experimental and computational advances in thermal boundary conductance and nanoscale thermal transport across solid interfaces, Adv. Funct. Mater. 30 (8) (2020) 1903857.
[58] W.A. Little, The transport of heat between dissimilar solids at low temperatures, Can. J. Phys. 37 (3) (1959) 334–349.
[59] E.T. Swartz, R.O. Pohl, Thermal resistance at interfaces, Appl. Phys. Lett. 51 (26) (1987) 2200–2202.
[60] Z. Shi, M. Barisik, A. Beskok, Molecular dynamics modeling of thermal resistance at argon-graphite and argon-silver interfaces, Int. J. Therm. Sci. 59 (2012) 29–37.
[61] H. Hu, Y. Sun, Effect of nanopatterns on Kapitza resistance at a water-gold interface during boiling: A molecular dynamics study, J. Appl. Phys. 112 (5) (2012) 53508.
[62] B.H. Kim, A. Beskok, T. Cagin, Molecular dynamics simulations of thermal resistance at the liquid-solid interface, J. Chem. Phys. 129 (17) (2008).
[63] B.Y. Cao, M. Chen, Z.Y. Guo, Rarefied gas flow in rough microchannels by molecular dynamics simulation, Chin. Phys. Lett. 21 (9) (2004) 1777–1779.
[64] G. Mohiuddin Mala, D. Li, Flow characteristics of water in microtubes, Int. J. Heat Fluid Flow 20 (2) (1999) 142–148.